

Revision 2

Adrianite, $\text{Ca}_{12}(\text{Al}_4\text{Mg}_3\text{Si}_7)\text{O}_{32}\text{Cl}_6$, a new Cl-rich silicate mineral from the Allende meteorite: An alteration phase in a Ca-Al-rich inclusion

Chi Ma^{1,*} and Alexander N. Krot²

¹Division of Geological and Planetary Sciences, California Institute of Technology, Pasadena, California 91125, USA

²Hawai'i Institute of Geophysics and Planetology, University of Hawai'i at Mānoa, Honolulu, Hawai'i 96822, USA

ABSTRACT

Adrianite (IMA 2014-028), $\text{Ca}_{12}(\text{Al}_4\text{Mg}_3\text{Si}_7)\text{O}_{32}\text{Cl}_6$, is a new Cl-rich silicate mineral and a Si, Mg analog of wadalite. It occurs with monticellite, grossular, wadalite and hutcheonite in altered areas along some veins between primary melilite, spinel and Ti,Al-diopside in a Type B1 FUN (Fractionation and Unidentified Nuclear effects) Ca-Al-rich inclusion (CAI), *Egg-3*, from the Allende CV3 carbonaceous chondrite. The mean chemical composition of type adrianite by electron probe microanalysis is (wt%) CaO 41.5, SiO₂ 27.5, Al₂O₃ 12.4, MgO 7.3, Na₂O 0.41, Cl 13.0, O=Cl -2.94, total 99.2, giving rise to an empirical formula of $(\text{Ca}_{11.69}\text{Na}_{0.21})(\text{Al}_{3.85}\text{Mg}_{2.88}\text{Si}_{7.23})\text{O}_{32}\text{Cl}_{5.80}$. The end-member formula is $\text{Ca}_{12}(\text{Mg}_5\text{Si}_9)\text{O}_{32}\text{Cl}_6$. Adrianite has the $I\bar{4}3d$ wadalite structure with $a = 11.981 \text{ \AA}$, $V = 1719.8 \text{ \AA}^3$, and $Z = 2$, as revealed by electron back-scatter diffraction. The calculated density using the measured composition is 3.03 g/cm^3 . Adrianite is a new secondary mineral in Allende, apparently formed by alkali-halogen metasomatic alteration of primary CAI minerals such as melilite, anorthite, perovskite, and Ti,Al-diopside on the CV chondrite parent asteroid. Formation of secondary Cl-rich minerals sodalite, adrianite, and wadalite during metasomatic alteration of the Allende CAIs suggests that the metasomatic fluids had Cl-rich compositions. The mineral name is in honor of Adrian J. Brearley, mineralogist at the University of

29 New Mexico, USA, in recognition of his many contributions to the understanding of
30 secondary mineralization in chondritic meteorites.

31

32 **Keywords:** adrianite, $\text{Ca}_{12}(\text{Al}_4\text{Mg}_3\text{Si}_7)\text{O}_{32}\text{Cl}_6$, new mineral, wadalite group, alteration
33 mineral, Ca-Al-rich inclusion, Allende meteorite, carbonaceous chondrite

34 -----

35 *E-mail: chi@gps.caltech.edu

36

37

INTRODUCTION

38 During a nanomineralogy investigation of the Allende meteorite, a new Cl-rich
39 silicate, $\text{Ca}_{12}(\text{Al}_4\text{Mg}_3\text{Si}_7)\text{O}_{32}\text{Cl}_6$ with the $I\bar{4}3d$ wadalite structure, named “adrianite”, was
40 identified in Ca-Al-rich inclusion (CAI) *Egg-3* (Fig. 1). The Allende meteorite, which fell at
41 Pueblito de Allende, Chihuahua, Mexico on February 8, 1969, is a CV3 (Vigarano type)
42 carbonaceous chondrite. Much work has been done on *Egg-3* (e.g., Meeker et al. 1983),
43 which is a coarse-grained igneous Type B1 FUN (Fractionation and Unidentified Nuclear
44 effects) CAI from Allende (Wasserburg et al. 2012).

45 Electron probe microanalysis (EPMA), high-resolution scanning electron microscope
46 (SEM) and electron back-scatter diffraction (EBSD) have been used to characterize
47 composition and structure of adrianite. Synthetic $\text{Ca}_{12}(\text{Al}_4\text{Mg}_3\text{Si}_7)\text{O}_{32}\text{Cl}_6$,
48 $\text{Ca}_{12}(\text{Al}_2\text{Mg}_4\text{Si}_8)\text{O}_{32}\text{Cl}_6$, or $\text{Ca}_{12}(\text{Mg}_5\text{Si}_9)\text{O}_{32}\text{Cl}_6$ have not been reported to date. We describe
49 here the first occurrence of $\text{Ca}_{12}(\text{Al}_4\text{Mg}_3\text{Si}_7)\text{O}_{32}\text{Cl}_6$ in a meteorite, as a new alteration
50 mineral in a CAI from a carbonaceous chondrite, and discuss its origin and significance for
51 secondary alteration processes that affected CV chondrites (e.g., Brearley and Krot 2012).
52 Preliminary results of this work are given by Ma and Krot (2014b).

53

54

MINERAL NAME AND TYPE MATERIAL

55 The new mineral and its name have been approved by the Commission on New
56 Minerals, Nomenclature and Classification of the International Mineralogical Association
57 (IMA 2014-028) (Ma and Krot 2014a). The mineral name is in honor of Adrian J. Brearley
58 (born 1958), mineralogist and cosmochemist at the University of New Mexico, in
59 recognition of his many contributions to meteorite mineralogy. He is one of the leading

60 authorities on alteration mineralogy studies of chondritic meteorites. The holotype specimen
61 is in section MQM803 in G. J. Wasserburg's Meteorite Collection of Division of Geological
62 and Planetary Sciences, California Institute of Technology, Pasadena, California 91125,
63 USA. This section also hosts holotype hutcheonite (IMA 2013-029; Ma and Krot 2014c).

64

65

OCCURRENCE AND ASSOCIATED MINERALS

66 *Egg-3* is a coarse-grained igneous Type B1 CAI with a core composed of normally-zoned
67 melilite ($\text{\AA}k_{46-76}$) and Ti,Al-diopside (in wt.%: 1.9–11.5 TiO_2 , 17.2–21.7 Al_2O_3), nearly pure
68 anorthite and Mg-spinel, and a mantle composed of gehlenitic melilite ($\text{\AA}k_{14-34}$) poikilitically
69 enclosing rounded inclusions of Ti,Al-diopside (in wt.%: 10.3–16.4 TiO_2 , 17.8–20.3 Al_2O_3) and
70 spinel (Fig. 1). The coarser spinel grains form a nearly continuous layer in the middle of the
71 melilite mantle. The CAI is surrounded by several rims (from inside outward) (1) a multilayered
72 Wark-Lovering rim (Wark and Lovering 1976) made of melilite+perovskite, Ti,Al-diopside, and
73 forsterite layers, (2) a forsterite-rich accretionary rim (Krot et al. 2001) composed of forsterite
74 overgrown by secondary ferroan olivine, (3) a fine-grained matrix-like rim largely composed of
75 ferroan olivine and nepheline, and (4) a discontinuous layer of salite-hedenbergite pyroxenes
76 and andradite.

77 The CAI experienced ion-alkali-halogen metasomatic alteration that largely affected its
78 primary melilite and resulted in formation of diverse secondary minerals depending on the
79 melilite composition (Brearley and Krot 2012). Gehlenite-rich melilite of the Wark-Lovering rim
80 is almost completely replaced by sodalite, nepheline, and Na-bearing (up to 1 wt% Na_2O)
81 plagioclase; grossular is minor (Figs. 2a, b). Spinel in the Wark-Lovering rim is enriched in FeO
82 (up to 10 wt.%). Gehlenite-rich melilite in the mantle is crosscut by grossular – Na-bearing
83 plagioclase veins (Figs. 2b, c). The plagioclase/grossular ratio in veins decreases towards the
84 CAI core. Åkermanite-rich melilite in the core is largely replaced by grossular, monticellite, Ti-
85 free Al-diopside, and wollastonite; secondary forsterite, kushiroite, wadalite, hutcheonite, and
86 adrianite are minor (Figs. 2d, e). The core anorthite experienced relatively minor alteration; it is
87 crosscut by veins of grossular, Na-rich melilite (up to 4.7 wt% Na_2O), kushiroite, and celsian
88 ($\text{BaAl}_2\text{Si}_2\text{O}_8$) (Figs. 2e, f). A trace amount of Ni-Fe-rich metal is present in the CAI core.

89 Adrianite occurs in contact with monticellite and grossular, plus nearby wadalite and
90 hutcheonite in alteration areas along some cracks between primary melilite, spinel and Ti,Al-

91 diopside in the core area of the CAI (Figs. 3–5). Hutcheonite ($\text{Ca}_3\text{Ti}_2(\text{SiAl}_2)\text{O}_{12}$) is a newly-
92 found garnet mineral (Ma and Krot 2014c).

93 X-ray elemental mapping reveals a zoned distribution of Na- and/or Cl-rich secondary
94 minerals: nepheline and sodalite occur largely in the peripheral part of the CAI, whereas wadalite
95 and adrianite are found exclusive in its core; the melilite mantle virtually lack Na- and Cl-rich
96 secondary minerals (Fig. 1).

97

98 APPEARANCE, PHYSICAL, AND OPTICAL PROPERTIES

99 Adrianite occurs as small, irregular, single crystals, 2–6 μm in size (Figs. 3–5), which are
100 the holotype material. Color, luster, streak, hardness, tenacity, cleavage, fracture, density, and
101 optical properties could not be determined because of the small grain size. Adrianite is non-
102 cathodoluminescent under the electron beam in an SEM. The calculated density is 3.03 g/cm^3
103 using the empirical formula.

104

105 CHEMICAL COMPOSITION

106 Backscattered electron (BSE) images were obtained using a ZEISS 1550VP field
107 emission SEM and a JEOL 8200 electron microprobe with AsB (angle selective backscatter) and
108 solid-state BSE detectors, respectively. Quantitative elemental microanalyses (3) were carried
109 out using the JEOL 8200 electron microprobe operated at 10 kV (for smaller interaction volume)
110 and 5 nA in focused beam mode. Analyses were processed with the CITZAF correction
111 procedure (Armstrong 1995) using the Probe for EPMA program from Probe Software, Inc.
112 Analytical results are given in Table 1. No other elements with atomic number greater than 4
113 were detected by WDS scans. The empirical formula (based on 32 oxygen atoms *pfu*) of type
114 adrianite is $(\text{Ca}_{11.69}\text{Na}_{0.21})(\text{Al}_{3.85}\text{Mg}_{2.88}\text{Si}_{7.23})\text{O}_{32}\text{Cl}_{5.80}$. This Cl-rich silicate is a new wadalite
115 group mineral with $\text{Si}^{4+} > \text{Al}^{3+}$ at tetrahedral sites in the structure. The general formula is
116 $\text{Ca}_{12}(\text{Si,Al,Mg})_{14}\text{O}_{32}\text{Cl}_6$. The ideal formula of the holotype material is $\text{Ca}_{12}(\text{Al}_4\text{Mg}_3\text{Si}_7)\text{O}_{32}\text{Cl}_6$.
117 The end-member formula is likely $\text{Ca}_{12}(\text{Mg}_5\text{Si}_9)\text{O}_{32}\text{Cl}_6$, which requires SiO_2 34.23, MgO 12.76,
118 CaO 42.59, Cl 13.46, $\text{O} = \text{Cl} - 3.04$, total 100.0 wt%. Associated wadalite has an empirical
119 formula of $(\text{Ca}_{11.58}\text{Na}_{0.09})(\text{Al}_{7.42}\text{Mg}_{1.29}\text{Si}_{5.39})\text{O}_{32}\text{Cl}_{5.66}$. Nearby primary melilite has an empirical
120 formula of $\text{Ca}_{2.00}(\text{Mg}_{0.51}\text{Al}_{0.45})(\text{Si}_{1.55}\text{Al}_{0.45})\text{O}_7$, and Ti,Al-diopside shows an empirical formula of
121 $\text{Ca}_{1.00}(\text{Mg}_{0.52}\text{Al}_{0.25}\text{Ti}_{0.18})(\text{Si}_{1.45}\text{Al}_{0.55})\text{O}_6$ with ~18 wt% Al_2O_3 and ~7 wt% TiO_2 .

122

123

CRYSTALLOGRAPHY

124

125

126

127

128

129

Single-crystal electron backscatter diffraction (EBSD) analyses at a sub-micrometer scale were performed using an HKL EBSD system on a ZEISS 1550VP SEM, operated at 20 kV and 6 nA in focused beam mode with a 70° tilted stage and in a variable pressure mode (25 Pa) (Ma and Rossman 2008, 2009). The EBSD system was calibrated using a single-crystal silicon standard. The structure was determined and cell constants were obtained by matching the experimental EBSD patterns with structures of wadalite, grossular, and mayenite.

130

131

132

The EBSD patterns can be indexed nicely by the $I\bar{4}3d$ wadalite structure and give a best fit using the wadalite structure from Feng et al. (1988) (Fig. 6), with a mean angular deviation of 0.31°, showing $a = 11.981 \text{ \AA}$, $V = 1719.8 \text{ \AA}^3$, and $Z = 2$.

133

134

135

136

137

138

139

The X-ray powder-diffraction data (in \AA for $\text{CuK}\alpha 1$, Bragg-Brentano geometry) are calculated from the cell parameters and the atomic coordinates of Feng et al. (1988) with the empirical formula from this study, using Powder Cell version 2.4. The strongest calculated lines are [d in \AA , intensity, I, scaled to 100 for the most intense peak, (h k l)] [2.679, 100, (4 2 0)], [2.446, 36, (4 2 2)], [2.995, 32, (4 0 0)], [1.661, 28, (6 4 0)], [1.601, 28, (6 4 2)], [4.891, 14, (2 1 1)], [2.187, 14, (5 2 1)], and [1.729, 14, (4 4 4)].

140

ORIGIN, SIGNIFICANCE AND IMPLICATIONS

141

142

143

Adrianite, $\text{Ca}_{12}(\text{Al}_4\text{Mg}_3\text{Si}_7)\text{O}_{32}\text{Cl}_6$, is the Si, Mg analogue of wadalite $\text{Ca}_{12}(\text{Al}_{10}\text{Si}_4)\text{O}_{32}\text{Cl}_6$. It is a new member of the wadalite group in the manyenite supergroup. Its end-member may be $\text{Ca}_{12}(\text{Mg}_5\text{Si}_9)\text{O}_{32}\text{Cl}_6$.

144

145

146

147

148

149

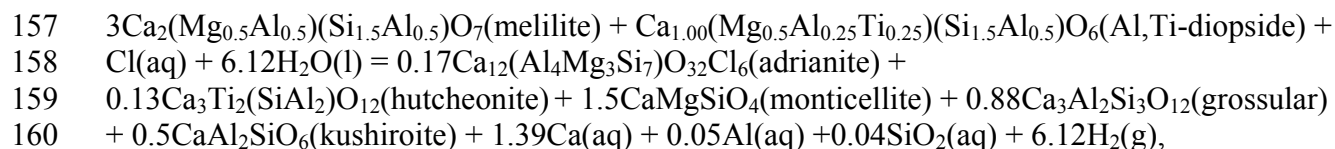
150

151

152

Adrianite is found only in altered regions of the Allende CAIs, in close association with secondary monticellite, grossular, hutchonite, and wadalite (Figs. 3–5). Mineralogical observations, thermodynamic analysis, and oxygen and ^{26}Al - ^{26}Mg isotope systematics of grossular, monticellite, and wollastonite in CV chondrites indicate that these minerals resulted from *in situ* alteration of the Allende CAIs during fluid-assisted thermal metamorphism of the CV chondrite parent asteroid below 600°C, ~3–4 Myr after CAI formation (Krot et al. 2007; Brearley and Krot 2012). Based on these observations, we infer that adrianite is also a secondary alteration product, formed by iron-alkali-halogen metasomatic alteration of the primary melilite, perovskite, and Ti,Al-diopside in the CAI on the Allende parent asteroid. *Egg-3* experienced

153 open-system, post-crystallization alteration that resulted in addition of Si, Na, Cl, and Fe, and
154 loss of Ca (Fig. 1); Al, Ti, and Mg were also mobile during the alteration. One possible reaction
155 to account for adrianite formation in *Egg-3*, based on simplified or end-member formulas, may
156 be expressed as:



161 where grossular, monticellite and kushiroite (CaTs, Ti-free Al-rich pyroxene) are among the
162 common secondary minerals, and melilite and Al,Ti-diopside are the major primary minerals that
163 were altered.

164 Secondary Cl-rich minerals identified in CAIs now include sodalite, chlormayenite
165 (previously known as “brearleyite”; Ma et al. 2011), wadalite, and adrianite. Each and every new
166 mineral identified in meteorites provide new information on forming conditions. Adrianite is one
167 of six new secondary minerals discovered in Allende CAIs, helping to reveal alteration processes
168 on the parent body.

169

170 **ACKNOWLEDGMENTS**

171 SEM, EBSD and EPMA were carried out at the Geological and Planetary Science
172 Division Analytical Facility, Caltech, which is supported in part by NSF grants EAR-0318518
173 and DMR-0080065. This work was also supported by NASA grant NNX12AJ01G. We thank
174 Mike Zolensky, Makoto Kimura, and associate editor Steve Simon for constructive reviews.

175

176 **REFERENCES CITED**

- 177 Armstrong, J.T. (1995) CITZAF: A package of correction programs for the quantitative electron
178 beam X-ray analysis of thick polished materials, thin films, and particles. *Microbeam*
179 *Analysis*, 4, 177–200.
- 180 Brearley, A.J. and Krot, A.N. (2012) Metasomatism in the early solar system: The record from
181 chondritic meteorites. In *Metasomatism and the Chemical Transformation of Rock –*
182 *Lecture Notes in Earth System Sciences*, 659–789.

- 183 Feng, Q.L., Glasser, F.P., Howie, R.A., and Lachowski, E.E. (1988) Chlorosilicate with the
184 $12\text{CaO}\cdot 7\text{Al}_2\text{O}_3$ structure and its relationship to garnet. *Acta Crystallographica*, C44, 589–
185 592.
- 186 Krot, A.N., Ulyanov, A.A., Meibom, A., and Keil, K. (2001) Forsterite-rich accretionary rims
187 around Ca, Al-rich inclusions from the reduced CV3 chondrite Efremovka. *Meteoritics &*
188 *Planetary Sciences*, 36, 611–628.
- 189 Krot, A.N., Yurimoto, H., Hutcheon, I.D., Libourel, G., Chaussidon, M., Petaev, M.I.,
190 MacPherson, G.J., Paque-Heather, J., and Wark., D. (2007) Anorthite-rich, igneous (Type
191 C) Ca,Al-rich inclusions from the CV carbonaceous chondrite Allende: Evidence for
192 multistage formation history. *Geochimica et Cosmochimica Acta* 71, 4342–4364.
- 193 Ma, C. and Krot, A.N. (2014a) Adrianite, IMA 2014-028. CNMNC Newsletter No. 21, August
194 2014, page 801. *Mineralogical Magazine*, 78, 797–804.
- 195 Ma, C. and Krot, A.N. (2014b) Discovery of a new Cl-rich silicate mineral,
196 $\text{Ca}_{12}(\text{Al}_4\text{Mg}_3\text{Si}_7)\text{O}_{32}\text{Cl}_6$: an alteration phase in Allende. 77th Annual Meteoritical Society
197 Meeting, Abstract #5432.
- 198 Ma, C. and Krot, A.N. (2014c) Hutcheonite, $\text{Ca}_3\text{Ti}_2(\text{SiAl}_2)\text{O}_{12}$, a new garnet mineral from the
199 Allende meteorite: An alteration phase in a Ca-Al-rich inclusion. *American Mineralogist*,
200 99, 667–670.
- 201 Ma, C. and Rossman, G.R. (2008) Barioperovskite, BaTiO_3 , a new mineral from the Benitoite
202 Mine, California. *American Mineralogist*, 93, 154–157.
- 203 Ma, C. and Rossman, G.R. (2009) Tistarite, Ti_2O_3 , a new refractory mineral from the Allende
204 meteorite. *American Mineralogist*, 94, 841–844.
- 205 Ma, C., Connolly, H.C., Beckett, J.R., Tschauer, O., Rossman, G.R., Kampf, A.R., Zega, T.J.,
206 Sweeney Smith, S.A., and Schrader, D.L. (2011) Brearleyite, $\text{Ca}_{12}\text{Al}_{14}\text{O}_{32}\text{Cl}_2$, a new
207 alteration mineral from the NWA 1934 meteorite. *American Mineralogist*, 96,
208 1199–1206.
- 209 Meeker, G.P., G.J Wasserburg, G.J., and Armstrong, J.T. (1983) Replacement textures in CAI
210 and implications regarding planetary metamorphism. *Geochimica et Cosmochimica Acta*,
211 47, 707–721.

- 212 Wark, D.A. and Lovering, J.F. (1976) Marker events in the early evolution of the solar system:
213 Evidence from rims on Ca-Al-rich inclusions in carbonaceous chondrites meteorites.
214 Proceedings of the Lunar and Planetary Science Conference, 8, 95–112.
- 215 Wasserburg G.J., Wimpenny, J., and Yin, Q.-Z. (2012) Mg isotopic heterogeneity, Al-Mg
216 isochrons, and canonical $^{26}\text{Al}/^{27}\text{Al}$ in the early solar system. Meteoritics & Planetary
217 Sciences, 47, 1980–1997.
- 218

219 Table 1. EPMA data for type adrianite and nearby wadalite in *Egg-3*.

220

Constituent (wt%) ^a	adrianite	wadalite	Probe Standard
	n=3 ^b	n=3	
SiO ₂	27.5(3) ^c	20.6(1)	grossular
Al ₂ O ₃	12.4(2)	24.0(5)	grossular
MgO	7.3(2)	3.3(4)	forsterite
CaO	41.5(4)	41.2(2)	grossular
Na ₂ O	0.41(3)	0.2(1)	albite
Cl	13.0(3)	12.73(3)	sodalite
-O	2.94(7)	2.87(1)	
Total	99.2	99.2	

221

222 ^a Detection limit at 99% confidence: 0.07 wt% Si, 0.07 wt% Al, 0.03 wt% Mg, 0.04 wt% Ca,
223 0.05 wt% Na, 0.04 wt% Cl.

224 ^b Number of point analyses.

225 ^c Standard deviation in bracket.

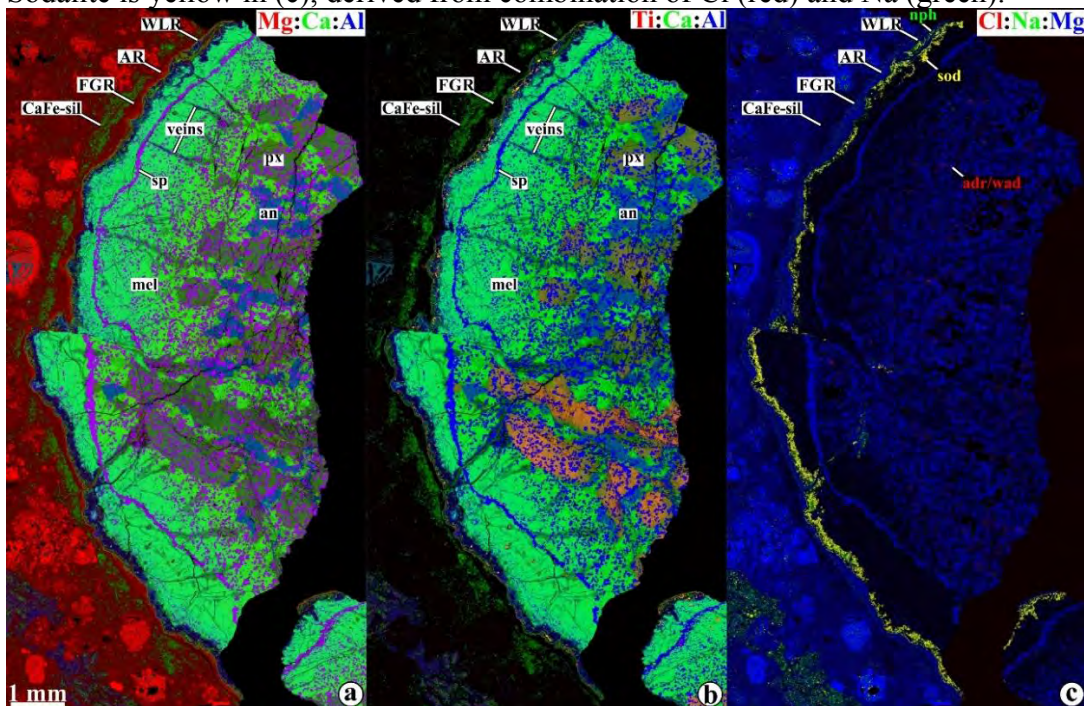
226

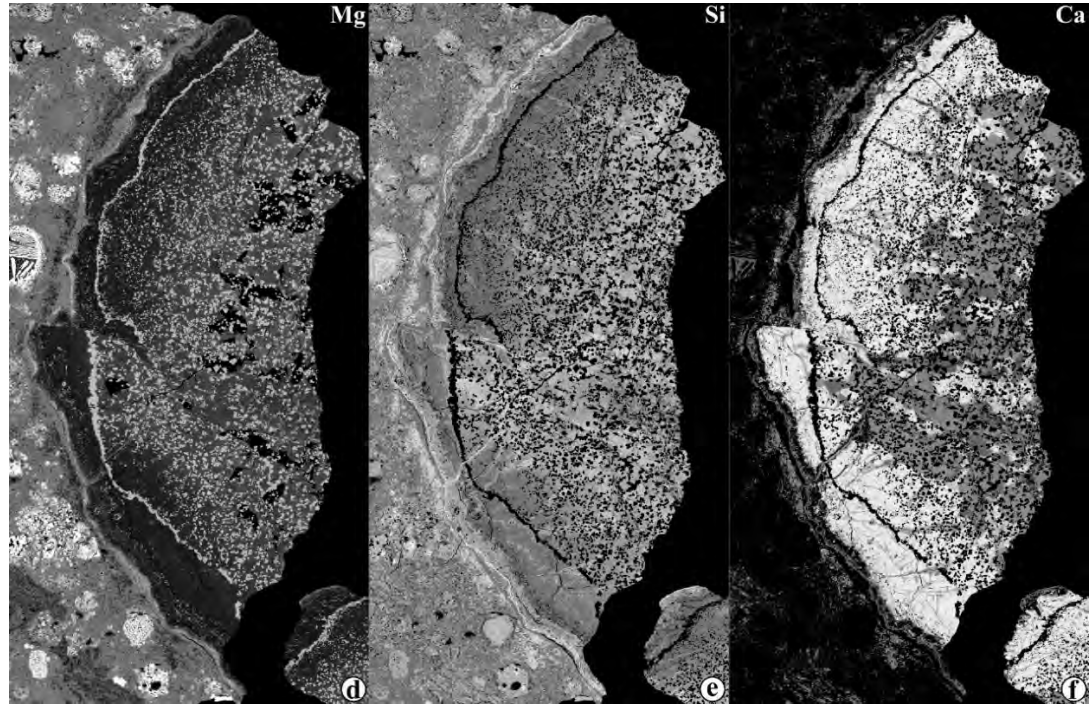
227

228

229 **Figure 1.** Combined x-ray elemental maps in (a) Mg (red), Ca (green) and Al (blue), (b) Ti (red),
230 Ca (green) and Al (blue), (c) Cl (red), Na (green) and Mg (blue), and x-ray elemental maps in (d)
231 Mg, (e) Si, and (f) Ca of the Allende Type B1 CAI *Egg-3*. The CAI experienced open-system
232 alteration that resulted in addition of Si, Na, Cl, and Fe, and loss of Ca. adr = adrianite; an =
233 anorthite; AR = forsterite-rich accretionary rim; CaFe-sil = layer of salite-hedenbergite
234 pyroxenes and andradite; FGR = fine-grained matrix-like rim; mel = melilite; nph = nepheline;
235 px = Ti,Al-diopside; sod = sodalite; sp = spinel; wad = wadalite; WLR = Wark-Lovering rim.
236 Sodalite is yellow in (c), derived from combination of Cl (red) and Na (green).

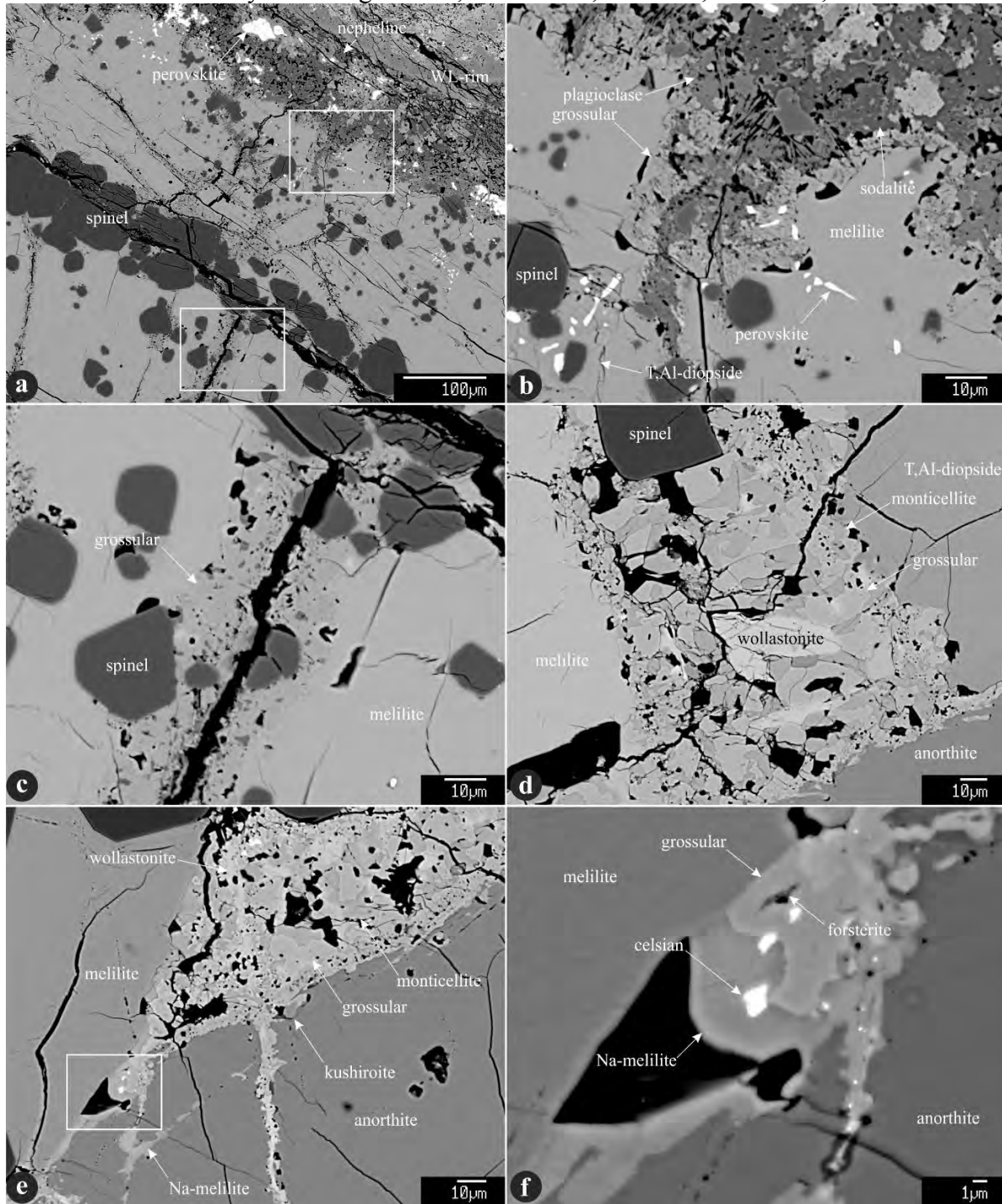
237





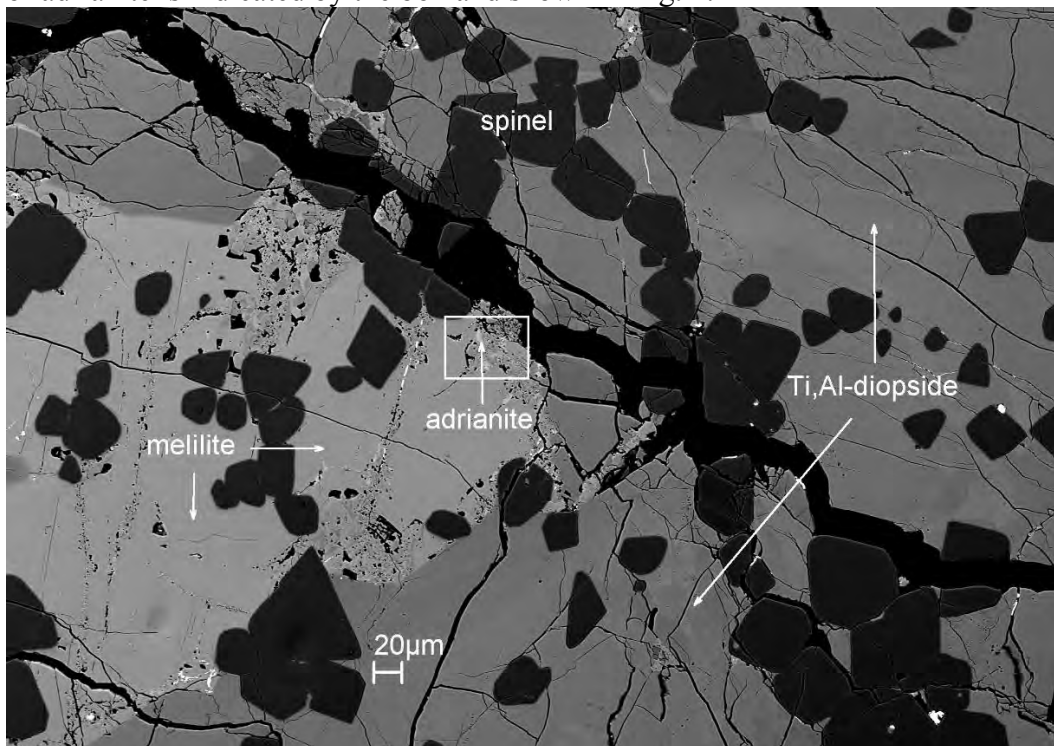
238

239 **Figure 2.** SEM BSE images showing secondary mineralization in different parts of *Egg-3*.
240 Regions outlined in “a” and “e” are shown in detail in “b, c” and “f”, respectively. (a–c)
241 Gehlenitic melilite near the Wark-Lovering (WL) rim is replaced by nepheline, sodalite, and Na-
242 bearing plagioclase. Gehlenitic melilite in the mantle is crosscut by plagioclase-grossular veins.
243 The abundance of anorthite in veins decreases towards the CAI core. (d–f) In the CAI core,
244 åkermanitic melilite is replaced by grossular, monticellite, wollastonite, and Ti-free Al-diopside.
245 Anorthite is crosscut by veins of grossular, Na-melilite, forsterite, kushiroite, and celsian.



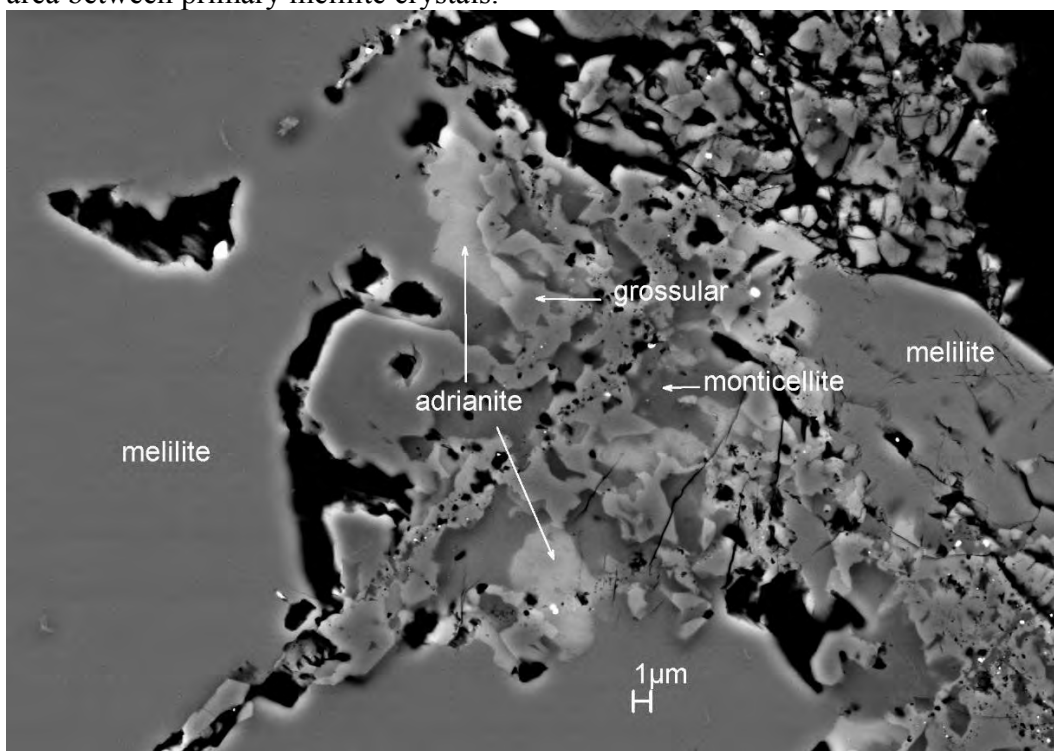
246
247

248 **Figure 3.** SEM BSE image showing part of the Type B1 CAI *Egg-3* in MQM803. The location
249 of adrianite is indicated by the box and shown in Fig. 4.



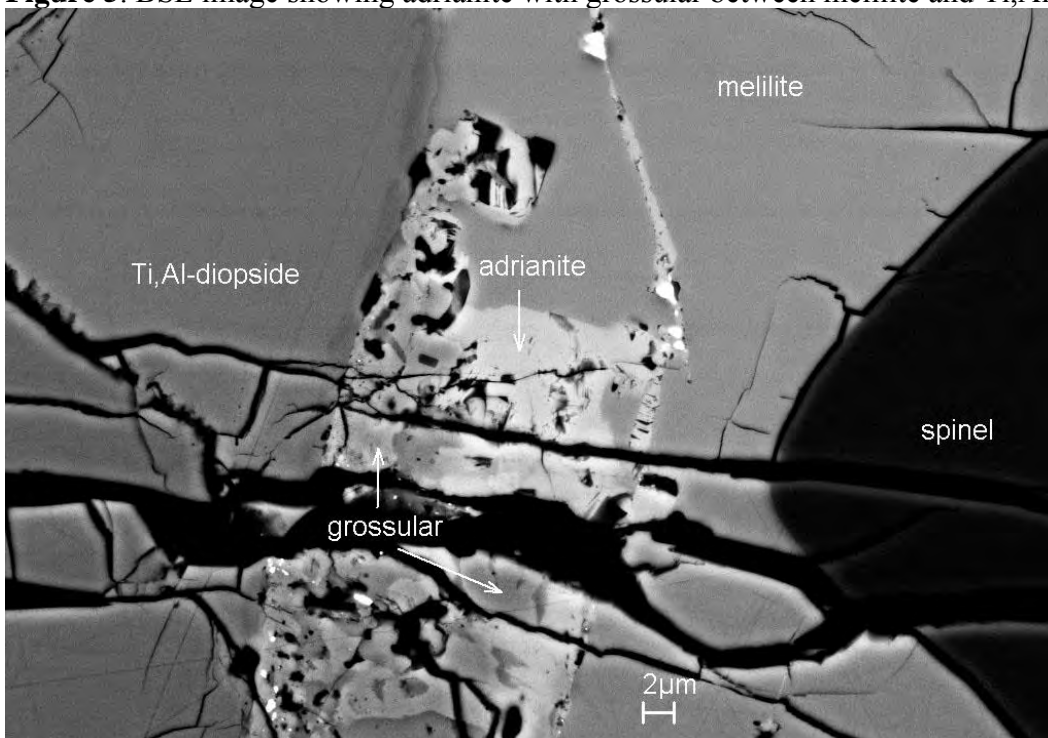
250
251
252
253

Figure 4. Enlarged BSE image revealing adrianite with grossular and monticellite in the altered
area between primary melilite crystals.



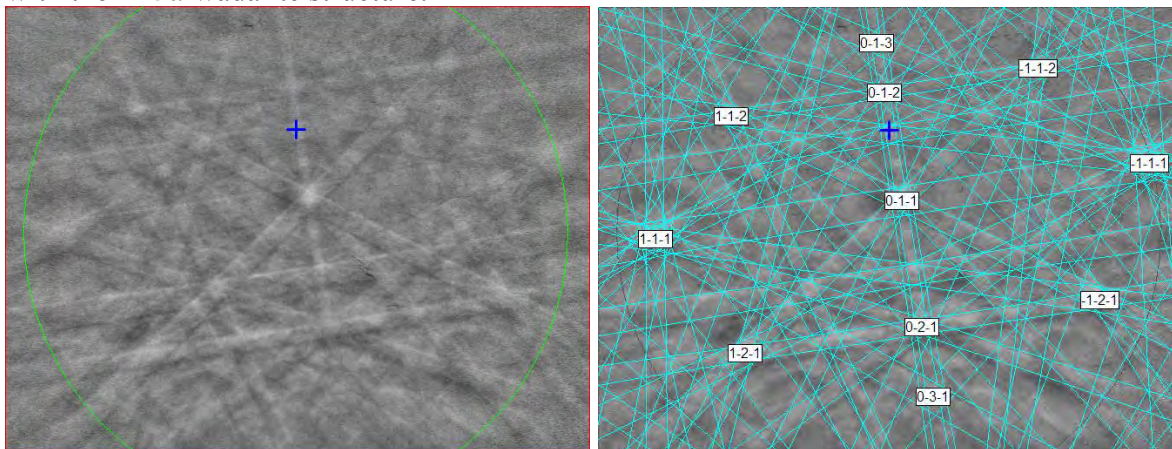
254
255

256 **Figure 5.** BSE image showing adrianite with grossular between melilite and Ti,Al-diopside.



257
258
259
260
261
262
263

Figure 6. (left) EBSD pattern of the adrianite crystal in Figure 2, and (right) the pattern indexed with the *I-43d* wadalite structure.



264
265
266